Available online at www.sciencedirect.com
ScienceDirect
Planetary and Space Science 55 (2007) 1541–1556
Planetary and Space Science
www.elsevier.com/locate/pss

The contribution of impulsive meteoritic impact vapourization to the Hermean exosphere

V. Mangano[a,b,*], A. Milillo[a], A. Mura[a], S. Orsini[a], E. De Angelis[a], A.M. Di Lellis[c], P. Wurz[d]

[a]*INAF-IFSI, via Fosso del Cavaliere 100, 00133 Roma, Italy*
[b]*CISAS-"G.Colombo", via Via Venezia 15, 35131 Padova, Italy*
[c]*AMDL srl, Roma, Italy*
[d]*Physics Institute, University of Bern, Sidlerstrasse. 5, CH-3012 Bern, Switzerland*

Accepted 25 October 2006
Available online 25 February 2007

Abstract

The exosphere of Mercury has been the object of many investigations and speculations regarding its composition, formation, depletion and dynamics. While vapourization of Mercurian surface materials by meteorite impacts has been often considered to be a less important contributor to the exosphere than other potential processes, larger objects coming from the Main Asteroid Belt could cause high local and transient enhancements in the density of the exosphere. Vapourization by such impacts is an almost stoichiometric process, and thus would contain valuable information about the surface composition. We investigate some exospheric effects of impact vapourization for meteorites with radii of 1, 10 cm, and 1 m, with particular reference to the missions that will explore Mercury during the next decade (MESSENGER and BepiColombo). Because of their higher probabilities, impacts of objects in the two smaller size ranges will surely occur during the lifetimes of the two missions. The enhancement of the exospheric density on the dayside of Mercury would be appreciable for the 10-cm and 1-m meteorites (some orders of magnitude, especially for Al, Mg, Si, and Ca). Such events could allow detection, for the first time, of refractory species like Al, Mg, and Si, which are expected to exist on the surface but have not yet been detected in the exosphere. Ca could be detectable in all cases, even if produced by impacting objects as small as 1 cm in radius. The lower exospheric background on the night side should allow easier identification of Na and K produced by impulsive events, even if their generally high background values make this eventuality less likely.

Keywords: Mercury exosphere; Impact vapourization; Meteorites; Exospheric dynamics

1. Introduction

In the last few years, two missions devoted to the exploration of Mercury have been approved: the NASA MESSENGER mission (Vaughan et al., 2006) and the ESA-JAXA BepiColombo mission (Balogh et al., 2000; Yamakawa et al., 2004; Langevin et al., 2005). MESSENGER was launched in August 2004 and should enter Mercurian orbit in 2011. The BepiColombo mission is scheduled to be launched in 2013, and to arrive at Mercury in 2019. The two missions have enormously revived interest in this fascinating planet.

One of the most intriguing aspects for investigation at Mercury is its behaviour under the extreme conditions of temperature gradients, solar radiation, and plasma precipitation. In particular, mechanisms of generating the Hermean exosphere, as well as its composition and configuration, could provide crucial insights into the planet's current state and its evolution. In fact, one of the main scientific objectives of the BepiColombo/Mercury Planetary Orbiter (BC/MPO), with periherm at 400 km and apoherm at 1500 km, is characterization of the planet's exosphere. To this end, an ultraviolet spectrometer

*Corresponding author. Tel.: +39 06 49934386; fax: +39 06 49934383.
E-mail address: valeria.mangano@ifsi-roma.inaf.it (V. Mangano).

0032-0633/$ - see front matter © 2007 Elsevier Ltd. All rights reserved.
doi:10.1016/j.pss.2006.10.008

(PHEBUS) and a particle-instrument package (SERENA) are included in the BC/MPO payload.

The first insights into the exospheric environment were provided by Mariner 10 measurements of H, He, and O during its fly-bys in 1974–1975 (Broadfoot et al., 1976); later, ground-based observations demonstrated the presence of Na (Potter and Morgan, 1985; 1990), K (Potter and Morgan, 1986), and Ca (Bida et al., 2000). Actual knowledge about the morphology of this extremely tenuous atmosphere is still very poor and significant volumes of new data will have to await the arrival of the spacecraft. Many theories and models have been constructed to make up for the lack of observational data and to try to understand the generation and dynamical evolution of the exosphere (e.g. Wurz and Lammer, 2003; Leblanc and Johnson, 2003; Killen and Ip, 1999). Among the many aspects of this issue, the roles played by the different sources and sinks in the dynamical balance of active exospheric processes are challenging topics, and they continue to be debated (see Milillo et al., 2005, for a review).

In the past, the process of impact vapourization caused by micrometeorites that come from the population present in the inner part of the Solar system has been generally considered as a secondary source of Hermean exospheric particles. For example, Killen et al. (2001) calculated that impact vapourization produces only about a quarter of the sodium in the exosphere, and that photon-stimulated desorption is consistently the dominant source process for this species. Wurz and Lammer (2003) estimate the micrometeoritic contribution to be one or two orders of magnitude smaller than other processes in their exospheric model. In particular, they use a Maxwellian-like energy distribution with a peak at 4000 K for the gas released by micrometeoritic impacts; they based this value on the experimental impact studies by Eichhorn (1978), in which the released gas was in the range of 2500–5000 K.

The contribution of vapourization by micrometeoroid impact to the global exosphere of Mercury still must be explored, particularly as it is expected to be the only process constantly active over the whole surface of the planet. In fact, other more effective processes, such as ion- and photo-sputtering and thermal desorption, are mainly active in specific regions of the dayside. In addition, they involve mainly volatile species, while impact vapourization is an almost stoichiometric process, meaning that it vapourizes all the species present in the regolith, even if with a higher percentage of volatile elements (Gerasimov et al., 1998); therefore, impact vapourization provides a contribution to the exosphere that is expected to contain valuable information about the surface composition.

Marchi et al. (2005) provided the distribution of impact probability as a function of impactor radius, up to objects of 100 m in radius. In particular, meteoritic impactors coming from the Main Asteroid Belt are expected to impact on Mercury as well. The contribution by these larger meteorites to the global Hermean exosphere, as investigated by Cremonese et al. (2005), is less than 1% of the total contribution due to the micrometeoroids as calculated by Cintala (1992); nevertheless, their impact could produce strong, localized, but temporary increase in the exospheric density, enriched of material coming from deeper layers. The impact frequency of such objects (especially in the lower size range) at Mercury is not negligible relative to the nominal duration of the BepiColombo mission (one year nominal plus one year extension).

We investigate what would happen should a meteoritic impact vapourization (MIV) event occur during the orbital phase of the BC/MPO mission. In particular, we estimate the density and composition of the cloud of impact vapour and, as a consequence, the detectability of each gaseous species already known or supposed to exist. The identification and detection of such an event would be particularly important on the night side, where the other exospheric refilling processes do not operate, and it would give additional information about the regolith's composition by way of remote sensing.

The models used for simulating the events are described in Section 2, and in Section 3, the evolution, configurations, and compositions of the clouds are examined for impactors of various sizes. Results are summarized and discussed in Section 4 and conclusions are presented in Section 5.

2. Models

To evaluate the vapour produced by a MIV event, we need to know: (1) the composition of the target soil; (2) the distribution and dynamical characteristics of the meteoroids; (3) a means of quantifying vapour production as a function of the parameters of projectiles, and (4) the dynamical evolution of the exospheric particles produced by the impact.

2.1. Soil composition

The paucity of observational data for the Hermean crustal composition leads to many uncertainties. While many efforts to collect data on that composition have been attempted (mainly from Earth-based spectroscopic observations), only a few constraints could be determined (Vilas, 1985; Emery et al., 1998, Sprague et al., 2000, 2002; Warell, 2004; Warell et al., 2006). Comparisons with laboratory emission spectra of different minerals have been performed (Sprague and Roush, 1998), and analogies with mature lunar highland soils have been hypothesized to give at least some general indications of its possible composition (Blewett et al., 2002). Obviously, a compositional heterogeneity over the whole planet surface is expected, but in general, a mixture of feldspar and pyroxene seems to match the spectral features quite well. In addition, we may find indications about the global composition of the planet from the models proposed by Goettel (1988) to account for the unusual high density of Mercury. Within the range of variation allowed by the heliocentric gradients in

temperature and pressure inside the primitive solar nebula, a refractory-rich model, a volatile-rich model, and a whole series of intermediate models can be hypothesized. Even though the refractory-rich model, which is one end member, is considered more probable than the other, an intermediate model is usually preferred, at least until a definitive value of the core's radius or the moment of inertia becomes available. Nevertheless, the uppermost layers of the surface are probably better described by the volatile-rich model. Hence, we use this model in our computations as being representative of the surface composition. Moreover, we add two other components: K and S (see Table 1).

The abundance of potassium is constrained by the optical measurements that discovered the existence of a potassium exosphere (Potter and Morgan, 1986). Although the exospheric abundance of K is found to be higher at Mercury than at the Moon, the Mercurian Na/K ratio is even larger by at least 1 or 2 orders of magnitude (Hunten and Sprague, 1997; Killen et al., 2004). The few available data have been included in the volatile-rich model preserving the average Na/K ratio of 100 (Table 1). K is an important target for investigation, since its exospheric abundance on Mercury is so different from the value detected at the Moon, and thus this discrepancy needs an explanation.

On the other hand, evidence for sulphur in the exosphere and, hence, on the surface would be important too, since it could give some constraints for different mineralogical models and also for the core composition. As there is no proof of the existence of S, the only abundances available are derived from models (Morgan and Killen, 1997); however, S is assumed to be present in the core to allow for the (partial) melting needed to explain the presence of the magnetic field. If we assume that at least a giant impact happened during the history of the planet (Benz et al., 1988; Cameron et al., 1988), then some S is expected to be present in the crust too.

2.2. Meteoritic distribution

The dynamic model of Marchi et al. (2005) investigates the likelihood of meter-sized objects hitting the Hermean surface. The origin of these meteoroids is the Main Belt, due to the 3:1 and the $\nu 6$ resonances, which change the meteoroids' orbital parameters and send them into the inner solar system. This model has been tested and calibrated for the case of the Earth (Morbidelli and Gladman, 1998).

Table 1
Composition of Mercury surface as derived from Goettel extreme volatile-rich model (1988) by adding S and K (in wt%)

Species	Abundance (wt%)
Al	1.911
Ca	2.151
Ti	0.083
Mg	19.193
Si	28.522
Fe	11.642
Na	0.582
O	35.304
S	0.578
K	0.034

The size distribution (shown in Fig. 1) gives the number of impacts per year and per meter into Mercury's surface as a function of impactor radius. In particular, we note that the impact of an object with radius in the range 0.5–1.5 m may happen twice every year; for objects of 5–15 cm the frequency rises to 2.3/day and objects in the range 1–2 cm should impact Mercury at a rate of 140/day. The velocity distributions for such impactors are shown in Fig. 2. According to Marchi et al. (2005), the velocities appear to be mostly concentrated in the range 20–70 km/s, with two peaks at approximately 30 and 40 km/s (their relative magnitude depending on the size of the objects). We choose the most probable velocity for each meteoroid size in our calculations. Hence, for the cases of 1 m and 10 cm, the assumed velocity is 40 km/s, while 1-cm meteoroids will impact at 30 km/s.

2.3. Vapour production

In thermodynamic calculations of vertical impacts by different meteoroids into lunar regolith, Cintala (1992) gave an estimation of the vapourized target volume (regolith) as a function of the projectile's velocity v_p and its radius r:

$$V_{\mathrm{vap}}(v_p, r) = \tfrac{4}{3}\pi r^3 (c + d v_{\mathrm{p}} + e v_p^2) \quad (1)$$

where c, d, and e are coefficients that depend on both the temperature of the soil (vapourization will be slightly easier for a higher-temperature regolith) and the composition of the projectile (higher-density impactors will generate greater shock stresses and thus vapourize more regolith).

We will use a surface temperature T_{s} of 400 K, which is typical at Mercury for a mid-longitude dayside location. A different soil temperature (the range being 100–700 K for the night side and the sub-solar point, respectively) will affect the result less than ±5% of the total vapour mass. Diabase will be used as the projectile material; it is a basaltic rock of about 3.0 g/cm^3, mainly made of plagioclase, pyroxene, and olivine; it should be a reasonable representation of the Main Belt meteoroids. We consider the projectile composition only for defining its density, which determines the coefficients in Eq. (1); we neglect its contribution to the vapour cloud, as it would represent only about 2–3% of the vapourized soil mass. The coefficients used in Eq. (1) are: $c = -0.848$, $d = -0.0889\,\mathrm{km^{-1}\,s}$ and $e = 0.0217\,\mathrm{km^{-2}\,s^2}$.

Laboratory experiments have shown that a target's porosity is more important than composition in determining the amount of vapour produced in an impact (Holsapple, 1993). Hence, the regolith density ρ used here is a combination of the densities of the regolith's components and its porosity. By assuming stoichiometric

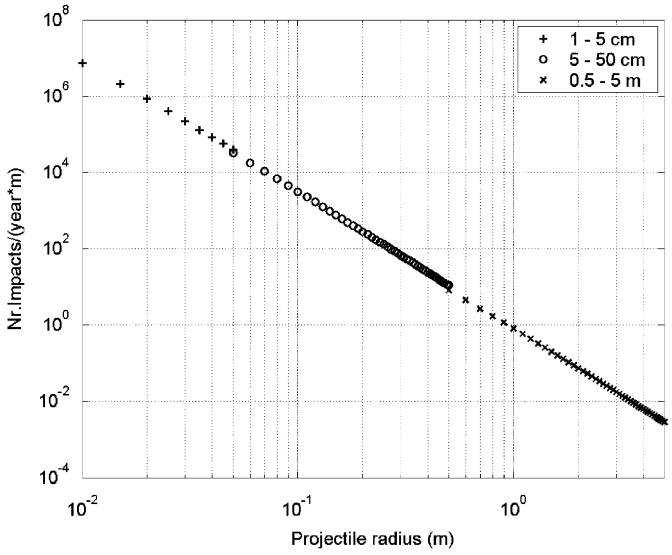

Fig. 1. Number of impacts (per year and per unit of projectile radius) over the whole surface of Mercury in the range 1 cm to 5 m.

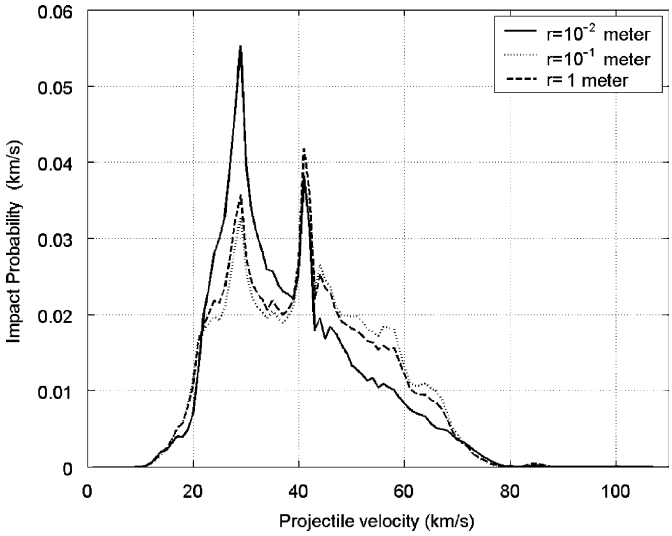

Fig. 2. The impact probability versus the velocity of the impacting object. Note how the profile changes with the size of the projectile, even though showing in any case two peaks at around 30 and 40 km/s.

vapourization and a regolith density 1.8 g/cm^3 (as used by Cintala, 1992), the total mass M of the vapour cloud can be computed. For a species x the number of atoms N_R generated by an impact is given by

$$N_R = \frac{\rho V_x \cdot N_A}{Z_x}, \quad (2)$$

where ρ is the regolith density, V_x the vapourized volume as derived from (1), Z_x is the atomic number of the species x, and N_A is the Avogadro constant. The parameter N_R will be used as an input in our MIV model (see next section), while the initial velocity of the particles will resemble a Maxwellian distribution with a characteristic temperature T_c of 4000 K (Eichhorn, 1978).

We consider the simplest case of impact perpendicular to the surface, which is expected to produce the highest volumes of vapour, and a nearly hemispherical vapour cloud. Different impact angles will produce less symmetric clouds and less vapour (Schulz, 1996).

2.4. MIV dynamic model

The spatial distribution of the neutral exospheric component produced by a MIV event is obtained by using the Monte-Carlo, single-particle model originally developed to simulate the particles released by ion sputtering (Mura et al., 2005). We first define a four-dimensional (4D), spherical grid (radius r from 1 to 2 R_M, latitude φ, longitude λ, and time t from 0 to 6000 s) of 24 × 24 × 24 ×

400 bins, respectively, and an associated 4D matrix Q_{ijkl}. We then trace the trajectories of about one million test-particles for each run using classical equations of motion, including gravity in the Mercurian reference frame, starting from the surface of Mercury at the impact point P_0 ($\varphi = 0$, $\lambda = 0$). The initial velocity v of the test-particle has random direction (with flat distribution over 2π) and intensity according to the Maxwellian distribution:

$$f(v) = \exp\left[-\frac{m_x v^2}{2kT_c}\right], \quad (3)$$

where m_x is the mass of the ejected particle x; the distribution is reproduced by using the rejection technique of Von Neumann (1951). A weight w is assigned to the test-particle, taking into account the total, real neutral source flux at P_0:

$$w(0) = \frac{N_R}{N_S} \quad (4)$$

where $N_S = 10^6$ is the number of simulated test-particles. A test-particle trajectory ends at the surface of the planet or when it is too far from the planet to be of further consequence (i.e., $10R_M$). Each time a test-particle crosses a grid cell *ijkl*, a quantity q is added to Q_{ijkl}:

$$q = w(t)\Delta t, \quad (5)$$

where Δt is the time elapsed inside the cell. After all trajectories have been simulated, the density in each grid cell *ijkl* is calculated by dividing Q_{ijkl} by the 4D volume of the cell.

3. Cloud formation

Given our model of the Hermean soil composition (see Section 2.1), we have analysed specific atomic species of the impact-generated cloud, including Na, Mg, Al, Si, S, K, Ca, and O. Only some of these elements have actually been detected, but they all are expected to exist, and upper values or density profiles are available (Killen and Ip, 1999; Wurz and Lammer, 2003).

We include in our analysis the effects of impacting objects with radii of 1 m, 10 and 1 cm on the surface of Mercury. In particular, we focus on the density variations at the BC/MPO periherm and apoherm altitudes (400 and 1500 km, respectively) and on the illumination conditions of the Hermean surface. In fact, on the full night side hemisphere the only refilling process expected to act is due to meteorites (even if, locally, planetary ion-sputtering process could take place, Delcourt et al., 2003), providing a lower average exospheric density than on the dayside. Hence, a MIV event would be identified more easily on the nightside because of its higher enhancement with respect to the local average value.

According to the exospheric model of Wurz and Lammer (2003), among the average density values of species of our interest, Na and K are expected to vary from dayside to nightside because of photon-stimulated desorption acting only on the dayside. In fact, if we consider the dayside average value as the sum of the contributions due to all refilling processes, we note that ion-sputtering is the only one other than impact vapourization that is expected to operate for Mg, Al, Si, S, Ca, and O, acting in specific regions and under specific boundary conditions. Hence, the sole process continuously refilling these species over the entire surface of the planet (both dayside and nightside) is micrometeorites impact vapourization. Therefore, the average density values for Mg, Al, Si, S, Ca, and O are assumed to be the same over the whole planet, regardless of the illumination conditions. Hence, these species will be treated separately from Na and K.

As an example of the evolution of the vapour cloud's shape and intensity, the Na cloud at different times t after impact ($t_{impact} = 0$ s) of a 1 m-sized object is shown in Fig. 3. Hereafter, we will use the model of Wurz and Lammer to have mean exospheric densities at the altitude of interest, for all investigated species. The density evolution of the same Na cloud at 400 and 1500 km above the impact point is plotted in Fig. 4 (for both dayside and nightside conditions). Because they are complementary, Figs. 3 and 4 should be viewed at the same time.

This MIV event produces a cloud that reaches 400 km altitude after 75 s (Fig. 3a), and it is visible above the average dayside exospheric density 100–900 s after the event. The enhancement is more than one order of magnitude at its maximum (about 4×10^{10} m^{-3} for $t \geqslant 200$ s, Fig. 3b). The expanding Na cloud arrives at 1500 km altitude at about $t = 550$ s, but on the dayside the increase is negligible with respect to the average value, and it would not be detectable in any case. During the night time, the lower average values allow the Na cloud to be detectable at both altitudes. The cloud reaches 400 km altitude after 75 s and it lasts for almost 3000 s; the enhancement is now more than three orders of magnitude. At 1500 km altitude the cloud becomes visible after 300 s and it grows for more than one order of magnitude; it disappears at about $t = 3000$ s.

Having described the specific case of Na, hereafter we will discuss all eight of the species in light of three different parameters: the intensification I of the cloud at its maximum; the duration of intensification Δt above background from the time of the initial enhancement; and the extension d of the cloud, defined as its angular width (calculated from the centre of the planet) at the location where the enhancement is one order of magnitude above the average exospheric value. These results are summarized in Table 3, and Fig. 5 shows the evolving cloud densities at 400 km resulting from the impact of a projectile 1 m in radius.

At 400 km (Fig. 5, top), the leading edge of the O cloud arrives 60 s after the impact; Mg, Al, Si, and S arrive after 75 s, and Ca after 90 s. The delays are longer as the atomic weight of the species increases. Mg, Al, Si, and Ca show the highest relative density increases at maximum, while the greatest duration is for Si and Ca, followed by Mg, Al, and

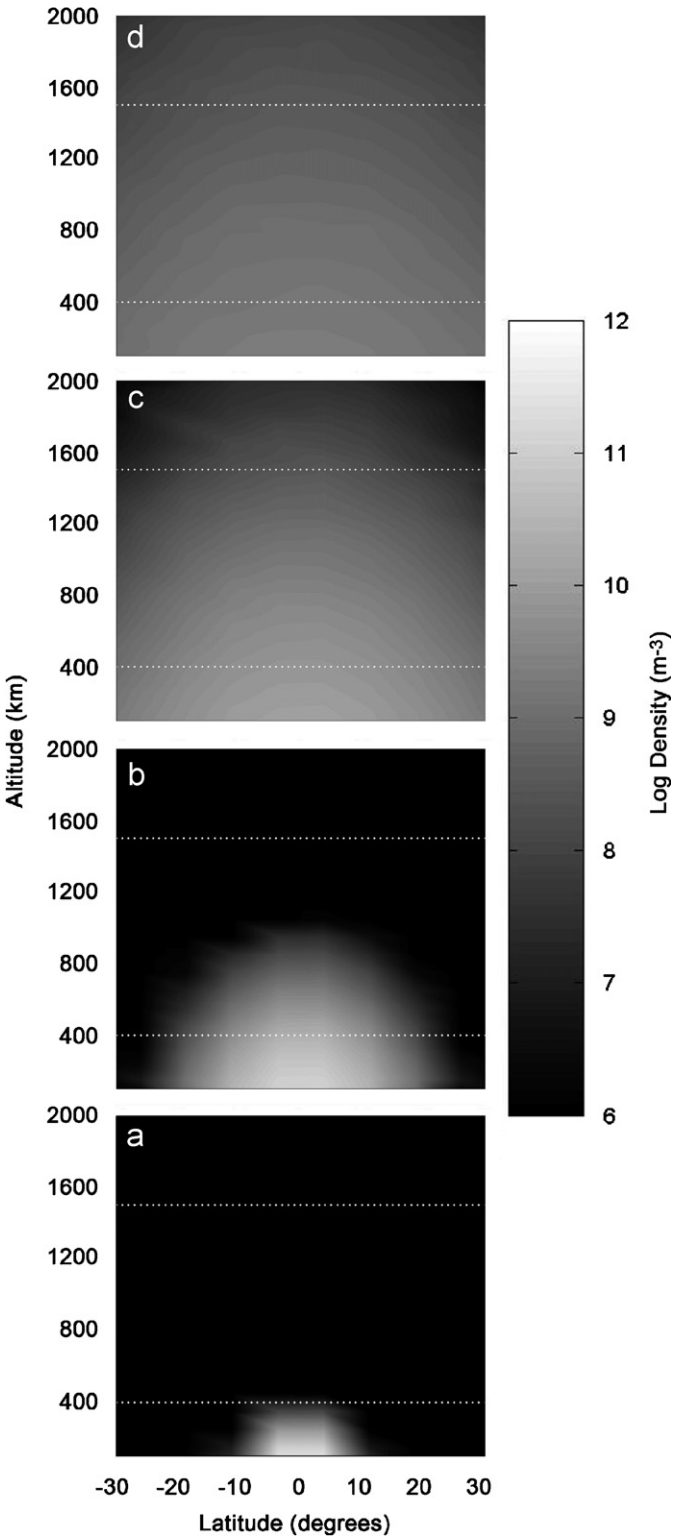

Fig. 3. Evolution of the sodium cloud with time for the case of 1 m (from bottom to top): (a) after 75 s the cloud reaches 400 km altitude; (b) after 200 s the enhancement at this altitude maximizes becoming more than one order of magnitude over local average value; (c) after 550 s the cloud reaches 1500 km altitude; (d) the highest intensification at this altitude is reached after 900 s. Dotted white lines represent the apoherm and periherm of BC/MPO (400 and 1500 km, respectively).

O. Considering the average densities at this altitude as listed in Table 2, this event would cause an enhancement of at least a factor of 10^4 for each of these species. In the cases of Na and K (Fig. 5, bottom) the nightside background appears to be two orders of magnitude weaker than that of the dayside. The enhancement for K is an order of magnitude on the dayside but three on the nightside. The durations of enhancement for Na and K are lower than for the others by a factor of 3 on the nightside and even less on the dayside. Cloud extensions are in the range 50–70° for the first group, between 0° and 20° for the dayside Na and K, and between 20° and 40° for the nightside Na and K.

Fig. 6 shows the same situation for 1500 km altitude. The O cloud reaches this altitude first after 250 s, because it is the lightest atom; after 300–400 s Mg, Al, Si, and S arrive. Because it is the heaviest of the studied species, Ca is also the slowest, requiring more than 400 s to attain 1500 km. The enhancement factors are in the range 10^3-10^6, and the durations are $\geqslant$5500 s. Once again, Ca is the most enhanced (a factor of 10^6 above the background values), with typical durations well above 6000 s. The Na and K enhancements, however, do not rise above the background values on the dayside. On the nightside they exceed the background exosphere by two orders and one order of magnitude, respectively; durations are in the range 2000–3200 s. Cloud extensions are in the range of 120–130° for the six species, and between 0° and 10° (dayside) and 70° and 100° (nightside) for Na and K.

Similar results are obtained for the case of a meteorite of 10 cm radius. The most probable velocity is still 40 km/s (Fig. 2), so the density versus time plots are exactly the same as before, but decreased by three orders of magnitude to correspond with the smaller impactor mass (Figs. 7 and 8). Mg, Al, Si and Ca are again the most enhanced elements, showing persistence in the range of 1900–3500 s (highest value for Ca) at 400 km (Fig. 7). The enhancements of the different species begin after the same time from impact found for the 1-m meteoroid, because the initial velocity of the expanding cloud is the same. Nevertheless, they start to become appreciable over the background exospheric density a short time after the cloud arrival. The density of the K cloud does not rise above the background value for either dayside or nightside; Na exceeds the background density, but only on the nightside. Cloud dimensions are in the range of 25–50°.

At 1500 km, the S enhancement remains below the average exospheric density, while the enhancements in the other species are appreciable only tens of seconds later than seen in the previous case (Fig. 8, bottom). The O cloud is the last to be appreciable and the first to vanish, with a poor enhancement of less than a factor of 10. Mg, Al, Si and Ca are once again the most enhanced, in this case by a factor of 100. Average exospheric densities of Na and K always remain above the cloud contribution in this case; hence, their enhancement is no longer visible on either the dayside or nightside. The duration of the overall density enhancement is more than 2200 s and the cloud dimension

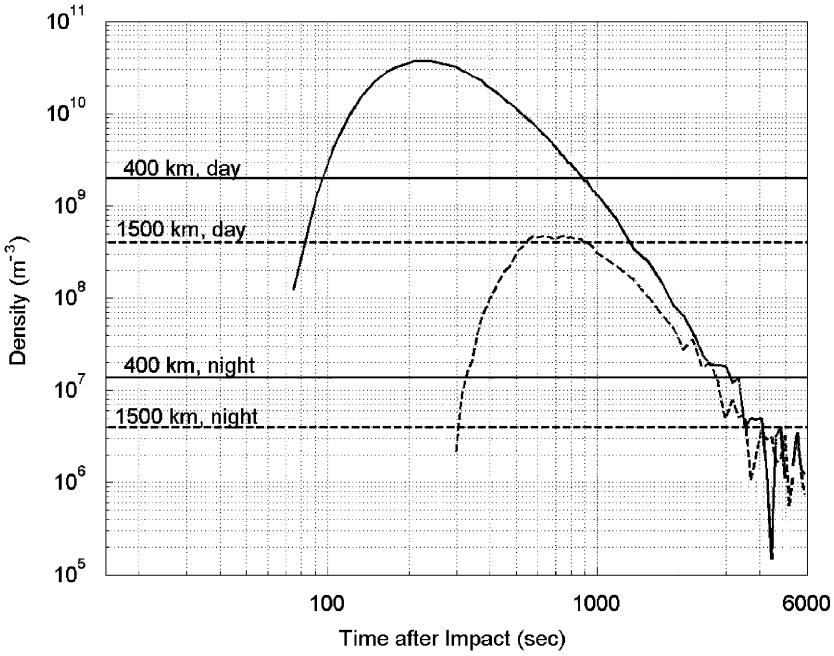

Fig. 4. Sodium enhancement versus time for an impact of 1 m-sized object at 400 km (solid line) and at 1500 km altitude (dashed line). The horizontal lines represent the night side and dayside mean Na densities at the two altitudes, according to the exospheric model of Wurz and Lammer (2003) (see Table 2).

Table 2
Average exospheric density values (in part/m^3) at 400 and 1500 km altitudes for the different species here analysed (from Wurz and Lammer model, 2003)

	Species density							
	Na[a]	Mg	Al	Si	S	K[a]	Ca	O
At 400 km	2×10^9 d 1.5×10^7 n	3×10^6	2.5×10^5	10^6	1.5×10^6	9×10^7 d 9×10^5 n	7×10^3	10^8
At 1500 km	4×10^8 d 4×10^6 n	4×10^5	3×10^4	1.5×10^5	2×10^5	2.5×10^7 d 2.5×10^5 n	1.5×10^3	1.5×10^7

[a]The two species Na and K show different daily and night average values (designated by d and n, respectively).

Table 3
The intensifications, durations and spatial dimensions of the enhancements for a MIV event at both altitudes of 400 and 1500 km in the cases of two meteorite sizes are shown: note, in particular, the case of 0.1 m as the most interesting. The extension d of the cloud is obtained by considering the spatial dimensions of the cloud where the density is one order of magnitude higher than the average value at that altitude

Meteorite of 1 m								
Altitude: 400 km								
Species	Na	Mg	Al	Si[a]	S	O	K	Ca[a]
Intensification I	>10 d $>10^3$ n	$>10^5$	$>10^5$	10^6	10^4	$>10^4$	$\sim$10 d $\sim10^3$ n	$>10^6$
Duration Δt	800 d 3000 n	>6000	>6000	$\gg6000$	~4000	~6000	700 d 2200 n	$\gg6000$
Extension d	20° d 40° n	60°	60°	60°	50°	50°	0° d 20° n	70°
Altitude: 1500 km								
Species	Na	Mg[a]	Al[a]	Si[a]	S	O	K	Ca[a]
Intensification I	~0 d $>10^2$ n	$>10^4$	$>10^4$	10^5	10^3	$>10^3$	/ d >10 n	10^6
Duration Δt	0 d	$\gg6000$	$\gg6000$	$\gg6000$	~5500	>6000	0 d	$\gg6000$

Table 3 (*continued*)

Meteorite of 1 m								
Extension d	~3200 n 10° d 100° n	120°	130°	120°	130°	120°	~2000n 0° d 70° n	130°
Meteorite of 0.1 m								
Altitude: 400 km								
Species	Na	Mg	Al	Si	S	O	K[b]	Ca
Intensification I	/ d ~3 n	~10^3 n	~10^3	10^3	10	>10	– –	<10^4
Duration Δt	0 d 300 n	1900	2000	~2500	800	~900	– –	3500
Extension d	–d 0° n	40°	50°	45°	25°	30°	–d –n	50°
Altitude: 1500 km								
Species	Na[b]	Mg	Al	Si	S[b]	O	K[b]	Ca
Intensification I	– –	<10^2	<10^2	10^2	–	<10	– –	>10^2
Duration Δt	– –	2700	~2200	~3200	–	1200	– –	3500
Extension d	–d –n	100°	70°	80°	20°	20°	–d –n	90°
Meteorite of 0.01 m								

[a]1 m Meteorite: the most enhanced species (10^4-10^6) and for longer time ($\gg 6000$).
[b]0.1 m Meteorite: some species go below the average values.

is in the range of 70–100° for Mg, Al, Si, and Ca. The cloud diameter is just 20° for S and O.

The most probable impact velocity for a meteoroid 1 cm in radius is 30 km/s, corresponding to the first peak of Fig. 2. Following Eq. (1), a lower impact velocity will result in production of less vapour per unit mass of projectile. Hence, as can be deduced from the trend from the 1- to 10-cm case, the vapour cloud would now always remain below the threshold of the average exospheric levels. Only Ca, due to its low background density, would be visible for a short time at 400 km altitude, with an enhancement of about a factor 3, a duration of 450 s, and a spatial dimension of just 10°.

4. Discussion

These results demonstrate a real probability that such clouds will be identified during the lifetime of a devoted mission to Mercury. In particular, we consider the characteristics of the BC/MPO probe, which will be in a polar orbit with a period T of two and half hours. The probability of detection of the cloud generated by a MIV event can be calculated as

$$P = [1 - (P_{\mathrm{nox}})^f] = [1 - (1 - P_x)^f] = [1 - (1 - P_\varphi \cdot P_\lambda)^f], \tag{6}$$

where f is the number of impacts derived from the frequency in Fig. 1, and P_x expresses the detection probability of a single event, which is composed of two terms: P_φ and P_λ, accounting for the latitude for the longitude contributions, respectively. They represent the 'coverage' in latitude and longitude along one polar orbit.

P_φ is composed of two parts: the first is the amplitude of the cloud with respect to a whole polar orbit; the second is the duration of the event with respect to the orbital period, giving the portion of an orbit that the probe can cover and arrive in time to detect the cloud enhancement. The sum of these two ratios gives the coverage in latitude (see Fig. 9).

P_λ is given by the portion of the planet covered by the cloud with respect to the half of the planet's surface as seen from the altitude of the probe. Hence, the two probabilities can be expressed as

$$P_\varphi = \frac{d + \omega \Delta t}{2\pi} = \frac{d}{2\pi} + \frac{\Delta t}{T}, \tag{7}$$

$$P_\lambda = \frac{d}{\pi},$$

where d is the angular width of the generated cloud, Δt is the duration of the intensification above the average exospheric density at the altitude of interest, and

$T = 9000$ s is the period of one orbit. P_φ must obey the condition: $P_\varphi \leqslant 1$.

We calculate the probability at the periherm and apoherm of the orbit, and consider the average value between the two as representative of the whole orbit. The probability is the sum of the two for the cases of Na and K, because they have different reference values on the dayside and nightside.

Since notable enhancements would be caused by the 1- and 10-cm meteoroids, we will consider them here. From the durations and spatial extents of the clouds that are expected to be generated, Eq. (6) provide the detection probabilities summarized in Tables 4 and 5. Even though the impact frequency of 1-m meteoroids is only 2 events/year, the large enhancements and spatial dimensions of the generated cloud result in a reasonable detection probability over one year; at 400 km altitude, the detection probability is in the range of 30–61% and it increases to 91–97% at 1500 km. This gives an average value in the range 60–79%. Na and K are not expected to be visible on the dayside,

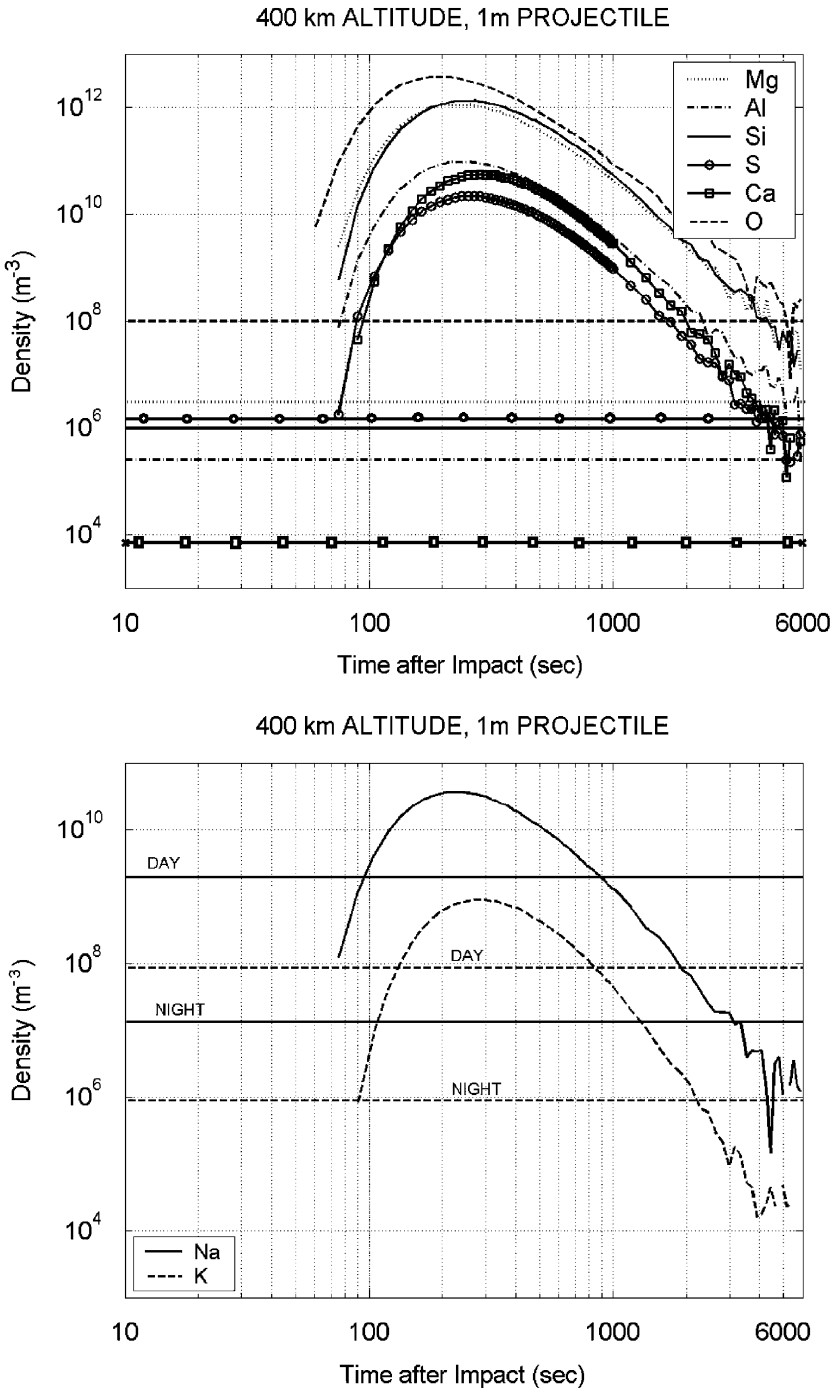

Fig. 5. Density versus time for an impacting object of 1 m radius, at 400 km altitude for the species whose mean density value does not change between day- and night-time (on top); separately, for Na and K (bottom). As in the fig. 4, horizontal lines represent the exospheric background for each species.

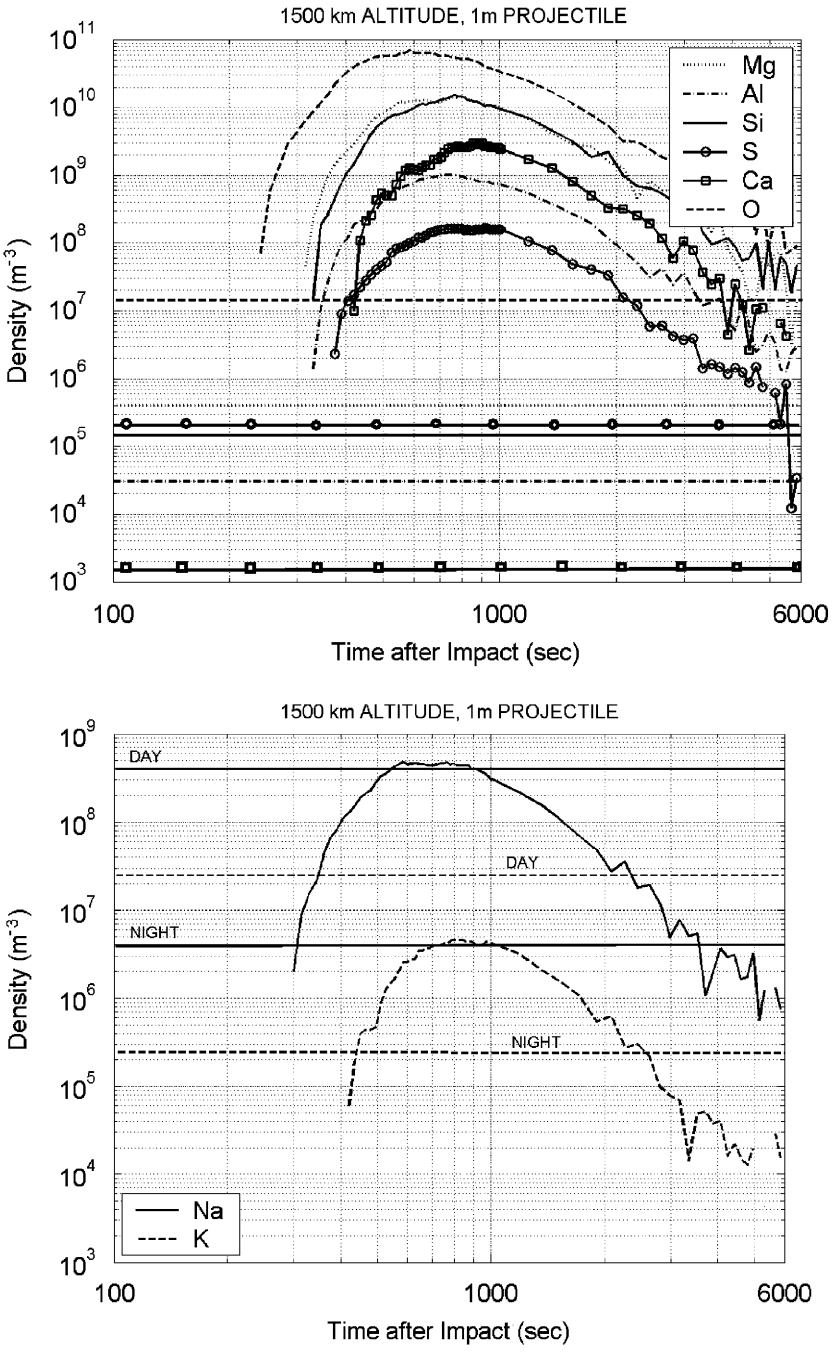

Fig. 6. Density versus time for an impacting object of 1 m radius, at higher altitude of 1500 km (same division among species as in previous figure).

while they reach almost 20% and 9% over one year on the nightside, respectively. The probabilities are generally quite low with respect to the other species because of the high background exospheric values on both sides of the planet. This is probably because Na and K are refilled not only by the micrometeoritic impact vapourization, but also by ion-sputtering, which seems to be particularly efficient.

The probabilities of detection for the 10-cm case also depend on the species under consideration due to the different values of cloud diameter and duration, but detection becomes likely after only one month. The first group of species has lower probabilities for S (detectable only at 400 km altitude) and higher for Mg, Al, and Si that reach almost 100% after one month. The Na and K probabilities are almost zero, while O reaches more than 5% after one day, and 82% after one month.

The smallest objects (1 cm in radius) with an impact frequency of 140/day should provide a contribution that

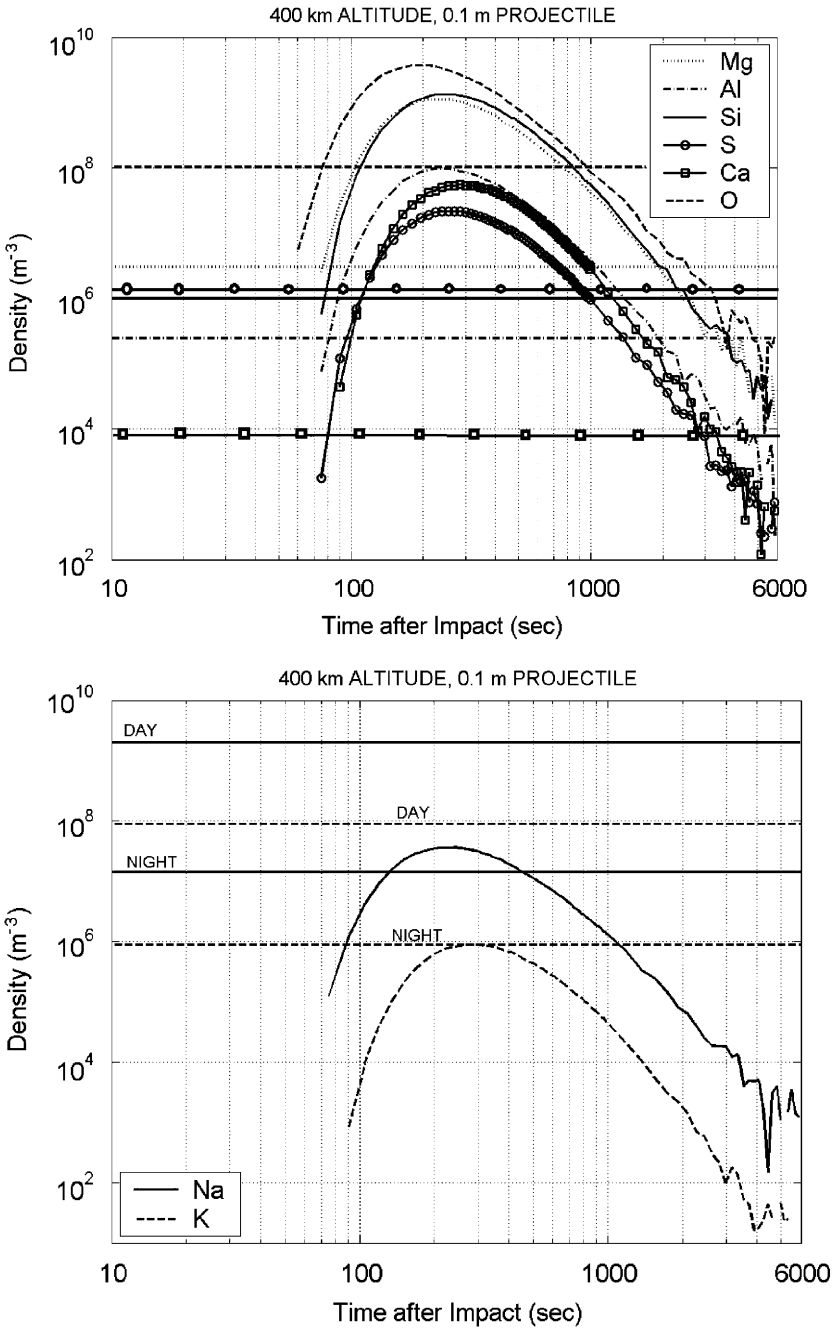

Fig. 7. Density versus time for an impacting object of 0.1 m radius, at 400 km altitude for the species whose mean density value does not change between day- and night-time (on top); separately, for Na and K (bottom). As in the previous two figures, horizontal lines represent the exospheric background for each species.

barely overcomes the average exospheric density, and could be detectable only by way of a calcium enhancement. With spatial dimension of 10° and duration of 450 s, the cloud produced by such an impact would give a probability of 1% over one day, 25% over one month, and 97% over one year. In this case, vapour production is undoubtedly shifting towards the non-impulsive processes, and towards continuous refilling by the much smaller and more abundant micrometeorites (Cremonese et al., 2005).

5. Conclusions

The previous two sections have demonstrated that large individual MIV events on Mercury should be observed during the BepiColombo mission because they would have reasonable probabilities of causing detectable, elemental enhancements in the planet's exosphere. Among the release processes active on Mercury, refractory species are released most efficiently by impact events; hence, MIV could be a valid mechanism by which species like Mg, Al, and Si

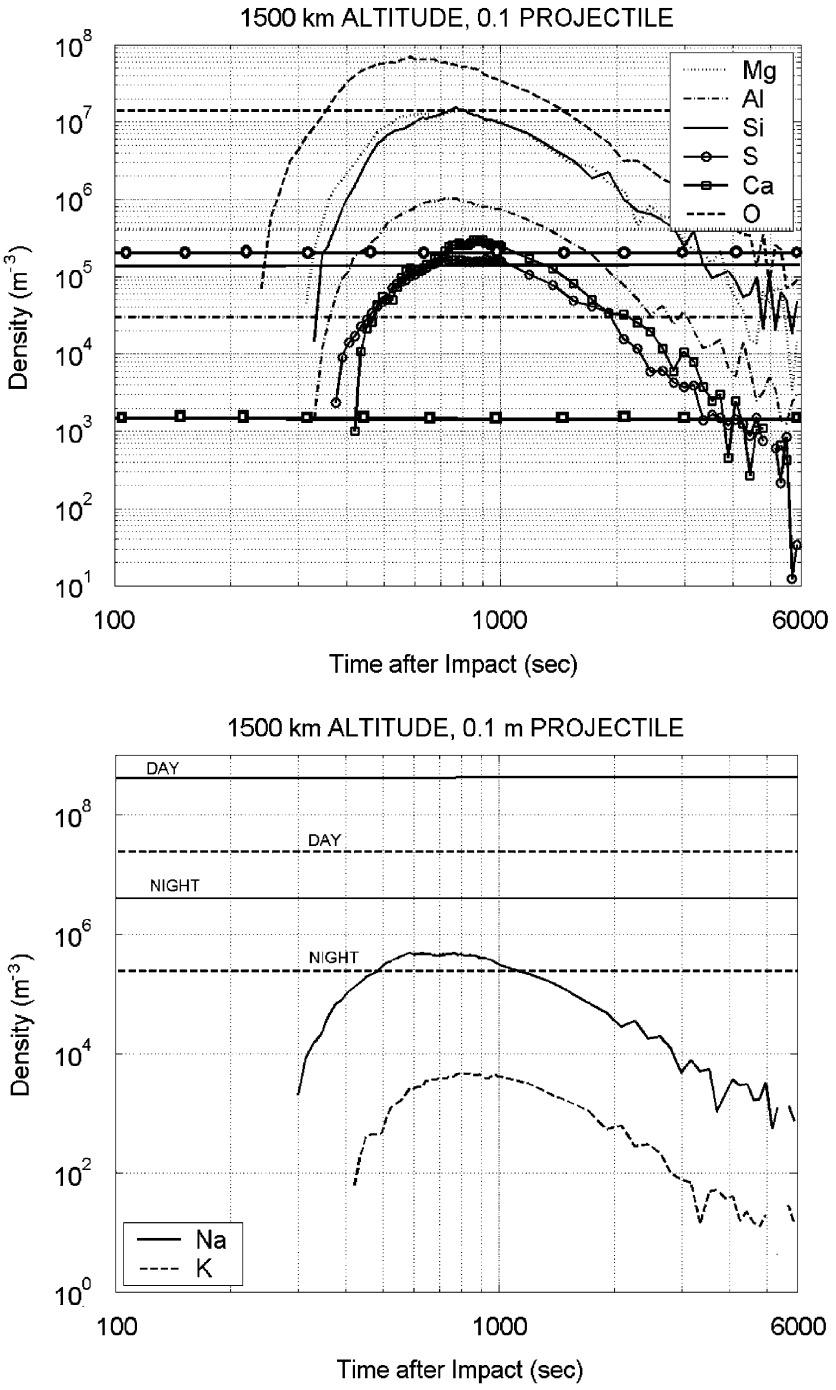

Fig. 8. Density versus time for an impacting object of 0.1 m radius, at higher altitude of 1500 km (same division among species as in previous figures). Note that now S, K and Na enhancements never approach mean exospheric values.

might be detected. The frequent impact of meteoroids 10 cm in radius makes them particularly interesting from our point of view.

On the other hand, the Na and K enhancements caused by MIV events offer few possibilities of being detected by the spacecraft, even on the nightside and in the most favourable case. This is mainly due to the high values of their average exospheric density that mask the main part of the MIV contribution. In particular, Na and K enhancements on the dayside would never be detectable for impactors smaller than 10 cm in radius. Even oxygen has a high exospheric reference density, but in this case the high abundance in the impact-produced cloud would permit a good probability of detection in the BepiColombo mission's lifetime.

A special point must be made for Ca: in this case the MIV event and the low background exospheric density assure a detectable enhancement and the production of a wide cloud. The detection probabilities are then very high,

even for the case of the 1-cm meteoroid. In fact, in this case Ca appears to be the only element still enhanced above the background values.

We split the produced cloud in its many different components, considering the point of view of an instrument devoted to the detection of a single species. Nevertheless, also global effects of such MIV events should be evaluated. In fact, the global density increase with respect to the background exosphere produced by a MIV event surely will be detectable. Such an event would be an interesting object of study in itself, in the context of gaining a better knowledge of transient exospheric effects as well as for determining the current cratering rate at Mercury.

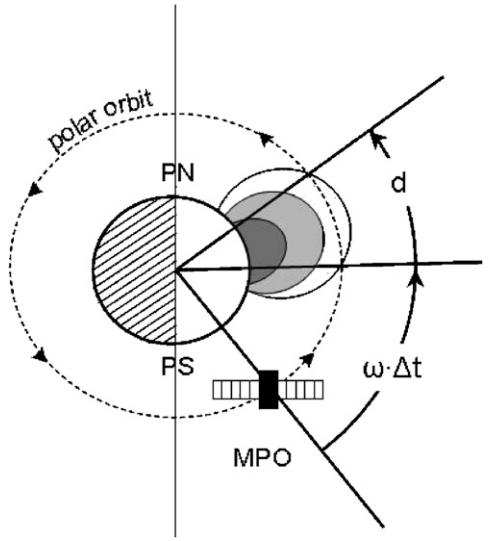

Fig. 9. A simple sketch of the BC/MPO polar orbit (circular, for simplicity) around Mercury (dashed line). If d is the cloud angular extension at the orbit altitude, the latitude contribution to probability will be the sum of d and that part of the orbit ($\omega \cdot \Delta t$) that the probe can cover and arrive still in time to detect the cloud enhancement.

The validity of this study is intended to be more qualitative as zero-order estimation than quantitative; in fact, there are many quantities that have had to be estimated and there are various neglected effects. Let us summarise them:

- The observational constraints of the composition of the Hermean surface are very poor and different surface composition models can be assumed. The model that we chose may not be the most representative.
- As already pointed out (see Section 2.3), we considered only vertical impacts, even if for a randomly oriented flux the most probable impact angle could be different from 90°. If all possible impact angles were included, the average vapourization efficiency would be lower (Schulz, 1996), resulting in clouds of smaller magnitude and hence lower detectabilities.
- We extended the Cintala's (1992) study, that separately considered vapour and melt production from the soil when small projectiles ($r < 10^{-3}$ m) impact the Hermean surface, to bigger meteorites. Given an adequate depth of regolith, the contributions to vapour and melt would not be very different over the impactor size considered here (Cintala, private communication).
- As the result of an impact, ejections of vapour together with melt and solid material will occur. Moreover, vapourized material is expected to be present not only in the atomic but also in molecular form. For example, it may happen that the oxygen is released, at least partly, in molecular form, O_2; conversely, it could be ejected as an oxide component, e.g. CaO as suggested by Killen et al. (2005). On the other hand, it could also be that part of the tetrahedral structure typical of the silicates (4 oxygen atoms and 1 silicon atom) maintains its original configuration when released as vapour. (The vapour temperature is 4000 K in this analysis, but it probably

Table 4
Probability to detect the cloud generated by a MIV event for a projectile of 1 m for all the considered species, for a circular orbit of 400 or 1500 km altitude (day and night probabilities are explicitly written for Na and K) and average values

Duration	Species							
	Na	Mg (%)	Al (%)	Si (%)	S (%)	O (%)	K	Ca (%)
400 km								
1 month	0.15% d + 0.9% n	5.6	5.6	6	3	4	0% d + 0.3% n	7.5
1 year	1.6% d + 9.4% n	50	50	53	30	40	0% d + 3.3% n	61
1500 km								
1 month	0% d + 3.5% n	20	25	20	18	18	0% d + 1.5% n	25
1 year	0% d + 29% n	93	97	93	91	91	0% d + 15% n	97
Average								
1 month	0.15% d + 2.2% n	12.8	15.3	15.3	13	10.5	11% d + 0.9% n	16.2
1 year	1.6% d + 19.2% n	71.5	73.5	73	60.5	60.5	0% d + 9.1% n	79

Table 5
Probability to detect the cloud generated by a MIV event for a projectile of 0.1 m for all the considered species, for a circular orbit of 400 or 1500 km and average values

Duration	Species							
	Na	Mg (%)	Al (%)	Si (%)	S (%)	O (%)	K	Ca (%)
400 km								
1 day	−d	15.5	21	21	5	6.8	−d	30
	−n						−n	
1 month	−d	99.3	99.9	99.9	77.8	87.8	−d	99.9
	−n						−n	
1500 km								
1 day	−d	20	22.5	27	—	4.7	−d	58
	−n						−n	
1 month	−d	99.8	99.9	99.9	—	76.3	−d	99.9
	−n						−n	
Average								
1 day	−d	17.7	21.7	24	0–5	5.7	−d	44
	−n						−n	
1 month	−d	99.5	99.9	99.9	0–77.8	82	−d	99.9
	−n						−n	

The probability of the most enhanced species (Mg, Al, Si and Ca) reaches almost the certainty after just one month. Na and K have no probability to be visible, neither at night.

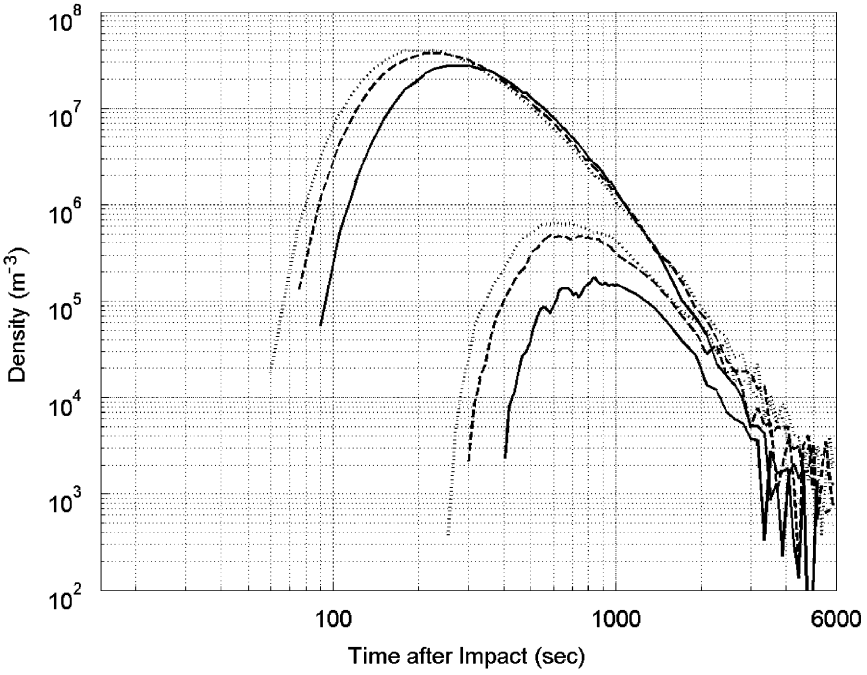

Fig. 10. Effects of cloud temperature on the density versus time plot, for the sodium component and for a 10 cm-radius projectile. Solid line for $T_c = 2500$ K, dashed line for $T_c = 4000$ K, dotted line for $T_c = 5000$ K. Upper curves are for 400 km altitude, bottom ones for 1500 km altitude.

was much hotter at the impact point.) In the first case, the results would be affected only by a scaling factor for the oxygen curve in our plots; in particular, this would result in an overestimation of the curves of both oxygen and bound species, while molecular species not considered here would be detectable in the exosphere instead. After some time, the molecules should dissociate, adding some energy to the exospheric components and permitting the involved species to reach higher altitudes (Killen et al., 2005). The occurrence of such cases would produce variations in the density profiles versus time of less than one order of magnitude; hence, it would not noticeably affect our results.

- We have not considered the processes like photoionization and charge-exchange that would decrease the cloud density; nevertheless, the typical lifetime of

such processes (e.g. Orsini et al., 2001; Killen and Ip, 1999) is much longer than the time scale of MIV events. Hence, we can assume that these processes are negligible.

- Because so much target material should be vapourized at these impact velocities, inclusion of the projectile's mass in the vapour cloud would change our results by a small amount (2–3%). This effect should be added to our vapour estimation, but it would not affect our conclusions in any appreciable sense.
- The temperature of the cloud is assumed to be 4000 K, but it is an unknown parameter. In any case, its value is expected to be in the range 2500–5000 K (Eichhorn, 1978). Higher values will result in a higher density enhancement and in a longer duration at BC/MPO altitudes; lower temperature will act in the opposite direction (Fig. 10). Even in this case, this would change the density enhancements by less than one order of magnitude.
- We choose a mean value of 400 K for the temperature of the soil, but the range between night- and dayside is 100–700 K. To choose one of these extreme values would imply maximum variations in the vapourized mass of only ±5%.
- All reference values for the dayside and nightside average exosphere are obtained from a model, hence they could be improved whenever more precise data become available or when the contributions from the different processes and their relative combinations become better known.
- The radiation pressure, which is known to act differently over different species, will surely affect the shape and local density of the clouds, depending on the impact position and on true anomaly angle. Such an effect cannot be quantified without loosing generality.

Nevertheless, even by considering all of those approximations in evaluating the effects of meteoritic impacts on the Hermean surface, the results of our analysis make us confident that MIV events during the BepiColombo mission could be identified and their vapour clouds studied as they occur. In fact, the noticeable increase of some species over the average exospheric density, the amplitude of the produced cloud, and the favourable detection probability of the MIV event all work in the direction of positive detections. This would aid in evaluating the surface composition and in assessing the refilling and escape mechanisms occurring at Mercury. Moreover, such events could help to detect for the first time several refractory species in the exosphere, and to increase our understanding of the still poorly known Ca exosphere.

Larger projectiles impacts vapourize the regolith deeper layers, which are less contaminated by space weathering (Hapke, 2001). The vapourized hemispherical volume could reach the dimension of meters, depending also on the density and porosity of the regolith. Hence, the detection of the vapourized soil could be the only way to remote sense the endogenous material.

The individual effects of the smallest objects analysed in our simulation are small compared to those of larger impactors, but, at a rate of 140 impacts/day, their global effects should be analysed further in the context of their contribution to the average exosphere. Moreover, over the lifetime of the BC/MPO mission, multiple MIV events could probably be detectable over the average exospheric density values. No asymmetry in the spatial distribution of those objects over the planet's surface is considered. Nevertheless, the possibility of asymmetries in the distribution of the infalling objects over the Hermean surface should be better investigated and not be excluded *a priori* (Marchi et al., 2005). In doing so, it would be necessary to include a local, time-dependent model of surface temperature and preferred impact velocity.

In the context of our study, the SERENA particle detector and the PHEBUS UV spectrometer onboard the BC/MPO module could have important roles in detecting the effects of MIV events (see ESA 'BepiColombo/MPO Payload Definition Document (PDD)', issue 4, revision 0–19 December 2003). In particular, SERENA is designed to work regardless of surface-illumination conditions, so it will also collect data on the nightside of the planet. As already discussed, Na and K enhancements could be detectable almost exclusively on the nightside of Mercury. Moreover, we cannot exclude the possibility of the detection of species whose dayside exospheric background has been underestimated.

Exospheric spatial inhomogeneities of refractory species with similar time scale could be generated also by ion-sputtering. Anyway, in this case the shape and intensity of the cloud would be significantly different (e.g. Mura et al., 2005). Furthermore, the generated cloud would be characterized by an energy spectrum reaching higher energies (Wiens et al., 1997). The energy resolution of SERENA will allow discriminating between these two processes.

Acknowledgements

The authors thank both referees for their valuable comments. We thank especially referee nr 2 for the effort spent in our paper.

References

Balogh, A., Bird, M., Blomberg, L., Bochsler, P., Bougeret, J.-L., Brückner, J., Iess, L., Guest, J., Langevin, Y., Milani, A.,. Sauvaud, J.-A, Schmidt, W., Spohn, T., von Steiger, R., Thomas, N., Torkar, K., Wänke, H., Wurz, P., 2000. BepiColombo-An interdisciplinary cornerstone mission to the planet Mercury. ESA-SCI(2000)1, Noordwijk, The Netherlands.

Benz, W., Slattery, W.L., Cameron, A.G.W., 1988. Collisional stripping of Mercury's mantle. Icarus 74, 516–528.

Bida, T.A., Killen, R.M., Morgan, T.H., 2000. Discovery of calcium in Mercury's atmosphere. Nature 404 (9), 159–161.

Blewett, D.T., Hawke, B.R., Lucey, P.G., 2002. Lunar pure anorthosite as a spectral analog for Mercury. Meteorit. Planet. Sci. 37, 1245–1254.

Broadfoot, A.L., Shemanky, D.E., Kumar, S., 1976. Mariner 10: Mercury atmosphere. Geophys. Res. Lett. 3, 577–580.

Cameron, A.G.W., Benz, W., Fegley, B., Slattery, W.L., 1988. The strange density of Mercury-Theoretical considerations. In: Vilas, F., Chapman, C.R., Matthews, M.S. (Eds.), Mercury. University of Arizona Press, Tucson, pp. 692–708.

Cintala, M.J., 1992. Impact-induced thermal effects in the lunar and Mercurian regoliths. J. Geophys. Res. 97, 947–973.

Cremonese, G., Bruno, M., Mangano, V., Marchi, S., Milillo, A., 2005. Release of neutral sodium atoms from the surface of Mercury induced by meteoroid impacts. Icarus 177, 122–128.

Delcourt, D.C., Grimald, S., Leblanc, F., Berthelier, J.-J., Millilo, A., Mura, A., Orsini, S., 2003. A quantitative model of planetary Na+ contribution to Mercury's magnetosphere. Ann. Geophys. 21, 1723–1736.

Eichhorn, G., 1978. Primary velocity dependence of impact ejecta parameters. Planet. Space Sci. 26, 469–471.

Emery, J.P., Sprague, A.L., Witteborn, F.C., Colwell, J.E., Kozlowski, R.W.H., Wooden, D.H., 1998. Mercury: thermal modelling and mid-infrared (5−12 μm) observations. Icarus 136, 104–123.

Gerasimov, M.V., Ivanov, B.A., Yakovlev, O.I., 1998. Physics and chemistry of impacts. Earth Moon Planet 80 (I. 1/3), 209–259.

Goettel, K.A., 1988. Present bounds on the bulk composition of Mercury-implications for planetary formation processes. In: Vilas, F., Chapman, C.R., Matthews, M.S. (Eds.), Mercury. University of Arizona Press, Tucson, pp. 613–621.

Hapke, B., 2001. Space weathering from Mercury to the asteroid belt. J. Geophys. Res. 106 (E5), 10039–10073.

Holsapple, K.A., 1993. The scaling of impact processes in planetary sciences. Annu. Rev. Earth Planet. Sci. 21, 333–373.

Hunten, D.M., Sprague, A.L., 1997. Origin and character of the lunar and Mercurian atmospheres. Adv. Space Res. 19, 1551.

Killen, R.M., Ip, W.-H., 1999. The surface-bounded atmosphere of Mercury and the Moon. Rev. Geophys. 37 (I. 3), 361–406.

Killen, R.M., Sarantos, M., Potter, A.E., Reiff, P., 2004. Source rates and ion recycling rates for Na and K in Mercury's atmosphere. Icarus 171, 1–19.

Killen, R.M., Bida, T.A., Morgan, T.H., 2005. The calcium exosphere of Mercury. Icarus 173 (I. 2), 300–311.

Langevin, Y., Schulz, R., Van Casteren, J., 2005. The BepiColombo Mission to Mercury. DPS meeting 37, 54.01. Bulletin of the American Astronomical Society, vol. 37, p. 741.

Leblanc, F., Johnson, R.E., 2003. Mercury's sodium exosphere. Icarus 164, 261–281.

Marchi, S., Morbidelli, A., Cremonese, G., 2005. Flux of meteoroid impacts on Mercury. Astron. Astrophys. 431 (I. 3), 1123–1127.

Milillo, A., Orsini, S., Wurz, P., Delcourt, D., Kallio, E., Killen, R.M., Lammer, H., Massetti, S., Mura, A., Barabash, S., Cremonese, G., Daglis, I.A., De Angelis, E., Di Lellis, A.M., Livi, S., Mangano, V., Torkar, K., 2005. Surface-exosphere-magnetosphere system of Mercury. Space Sci. Rev. 117 (I. 3), 397–444.

Morbidelli, A., Gladman, B., 1998. Orbital and temporal distributions of meteorites originating in the asteroid belt. Meteorit. Planet. Sci. 33, 999–1016.

Morgan, T.H., Killen, R.M., 1997. A non-stoichiometric model of the composition of the atmospheres of Mercury and the Moon. Planet. Space Sci. 45, 81–94.

Mura, A., Orsini, S., Milillo, A., Delcourt, D., Massetti, S., De Angelis, E., 2005. Dayside H^+ circulation at Mercury and neutral particle emission. Icarus 175, 305–319.

Orsini, S., Milillo, A., De Angelis, E., Di Lellis, A.M., Zanza, V., Livi, S., 2001. Remote sensing of Mercury's magnetospheric plasma environment via energetic neutral atoms imaging. Planet. Space Sci. 49, 1659–1668.

Potter, A.E., Morgan, T.H., 1985. Discovery of Na in the atmosphere of Mercury. Science 229, 651–653.

Potter, A.E., Morgan, T.H., 1986. Potassium in the atmosphere of Mercury. Icarus 67, 336–340.

Potter, A.E., Morgan, T.H., 1990. Evidence for magnetospheric effects on the sodium atmosphere of mercury. Science 248, 835–838.

Schulz, P.H., 1996. Effect of impact angle on vaporization. J. Geophys. Res. 101 (E9), 21117–21136.

Sprague, A.L., Roush, T.L., 1998. Comparison of laboratory emission spectra with Mercury telescopic data. Icarus 133, 174–183.

Sprague, A.L., Deutsch, L.K., Hora, J., Fazio, G.G., Ludwig, B., Emery, J., Hoffmann, W.F., 2000. Mid-infrared imaging of (8.1–12.5 μm) Mercury. Icarus 147, 421–432.

Sprague, A.L., Emery, J.P., Donaldson, K.L., Russel, R.W., Lynch, D.K., Mazuk, A.L., 2002. Mercury: mid-infrared (3–13.5 μm) observations show heterogeneous composition, presence of intermediate and basic soil types, and pyroxene. Meteorit. Planet. Sci. 37, 1255–1268.

Vaughan, R.M., Leary, J.C., Conde, R.F., Dakermanji, G., Ercol, C.J., Fielhauer, K.B., Grant, D.G., Hartka, T.J., Hill, T.A., Jaskulek, S.E., McAdams, J.V., Mirantes, M.A., Persons, D.F., Srinivasan, D.K., 2006. Return to Mercury: the MESSENGER spacecraft and mission. Institute of Electrical and Electronics Engineers (IEEE) Aerospace Conference, Big Sky, MT, 15.

Vilas, F., 1985. Mercury: absence of crystalline Fe in the regolith. Icarus 64, 133–138.

Von Neumann, J., 1951. Various techniques used in connection with random digits. National Bureau of Standard Applied Mathematics Series, vol. 12, pp. 36-38.

Warell, J., 2004. Properties of the Hermean regolith: IV. Photometric parameters of Mercury and the Moon contrasted with Hapke modelling. Icarus 167, 271–286.

Warell, J., Sprague, A.L., Emery, J.P., Kozlowski, R.W.H., Long, A., 2006. The 0.7−5.3 μm IR spectra of Mercury and the Moon: evidence for high-Ca clinopyroxene on Mercury. Icarus 180, 281–291.

Wiens, R.C., Burnett, D.S., Calaway, W.F., Hansen, C.S., Kykkem, K.R., Pellin, M.L., 1997. Sputtering products of sodium sulfate implications for Io's surface and for sodium-bearing molecules in the Io torus. Icarus 128, 386–397.

Wurz, P., Lammer, H., 2003. Monte-Carlo simulation of Mercury's exosphere. Icarus 164, 1–13.

Yamakawa, H., Ogawa, H., Kasaba, Y., Hayakawa, H., Mukai, T., Adachi, M., 2004. Current status of the BepiColombo/MMO spacecraft design. Adv. Space Res. 33, 2133–2141.